Cement & Concrete Composites 32 (2010) 411–420

Contents lists available at ScienceDirect

Cement & Concrete Composites

journal homepage: www.elsevier.com/locate/cemconcomp

Corrosion protection performance of High Performance Fiber Reinforced Cement Composites as a repair material

Koichi Kobayashi [a,*], Takahiro Iizuka [b], Hoshito Kurachi [c], Keitetsu Rokugo [a]

[a] Department of Civil Engineering, Gifu University, Yanagido 1-1, Gifu 501-1193, Japan
[b] Technology Research and Development Department, Central Japan Railway Company, 1545-33 Ohyama, Komaki 485-0801, Japan
[c] Nagoya Branch, Takenaka Civil Engineering & Construction Co., Ltd., Nishiki 1-18-12, Naka-ku, Nagoya 460-0003, Japan

ARTICLE INFO

Article history:
Received 12 May 2009
Received in revised form 10 March 2010
Accepted 14 March 2010
Available online 17 March 2010

Keywords:
HPFRCC
Fiber content
Patch repair
Surface coating
Chloride-induced corrosion
Durability

ABSTRACT

This paper regards the corrosion protection performance of High Performance Fiber Reinforced Cement Composites (HPFRCC) as a repair material. For the purpose of improving workability, the volumetric fiber content in HPFRCC was decreased from its usual rate of 1.5% to as low as 0.75%. The applicability of HPFRCC as a repair material for preventing steel corrosion was investigated using specimens that simulated either surface coating repair or patch repair. The results can be summarized as follows: Patch repair with HPFRCC to depths beyond the backside of the reinforcement effectively suppressed chloride penetration and prevented reinforcement corrosion, whereas surface coating with HPFRCC could not prevent corrosion of the steel in the RC substrate. As long as the fiber content is set so that only fine cracks are formed under service conditions, differences in fiber content did not affect the corrosion preventing performance of HPFRCC as a repair material.

1. Background

Reinforced concrete is an intrinsically durable composite system in which highly alkaline concrete covers corrosion-susceptible reinforcing steel. The alkaline environment supports the formation of a tight and thin passive film on the steel, which prevents corrosion. However, when chloride ions penetrate the cover concrete and reach the steel surface, the passive film becomes damaged. In the presence of sufficient moisture and oxygen, and if an electrical circuit is formed, the steel starts to corrode, which can lead to deterioration of the RC structure performance.

To prevent the ingress of aggressive agents into the concrete, it is effective to decrease the diffusion coefficient of these agents by reducing the water–cement ratio. However, RC members are usually designed so that some bending cracks are accommodated. In addition, RC members made with low water–cement ratio concrete are prone to cracking due to larger shrinkage of the concrete and higher steel-to-concrete ratios. Chloride, moisture, and oxygen can more easily reach the reinforcing steel through these cracks, resulting in the corrosion of reinforcing steel. Once such deterioration occurs in a RC member, it must be repaired appropriately. Common repair methods for structures deteriorated by chloride-induced corrosion include patch repair using polymer cement mortar (PCM), and surface coating using resin. Often, however, the repaired concrete suffers deterioration, which is mostly caused by physical and electrochemical incompatibilities between the substrate concrete and the repair material.

High Performance Fiber Reinforced Cement Composites (HPFRCC), which are composed of a cement-based matrix and short reinforcing fibers, exhibit multiple fine cracks and pseudo strain-hardening characteristics under uni-axial tensile stress [1]. While the material allows numerous tensile cracks to be generated, it is expected to have high impermeability to chloride, moisture, and oxygen gas because the crack widths are small. Besides, its matrix composition is similar to that of mortar with low water–cement ratio and it is highly ductile. HPFRCC is therefore suitable as a repair material, as it provides high bond strength to the substrate and high crack-bridging capacity [2]. HPFRCC is expected to be highly applicable as a patch repair or surface coating material for the repair and the preventive maintenance of structures that have already deteriorated or will deteriorate due to steel corrosion [3–7]. However, research on HPFRCC has been mainly focused on its mechanical performances such as tensile strength and ductility, and its applicability for the repair and preventive maintenance (collectively referred to below as "repair") against steel corrosion has not been investigated sufficiently yet.

The mechanical and physical properties of HPFRCC must be investigated before applying it as a repair material, but cost and

* Corresponding author. Tel.: +81 58 293 2470; fax: +81 58 293 2398.
E-mail address: ko2ba@gifu-u.ac.jp (K. Kobayashi).

0958-9465/$ - see front matter © 2010 Elsevier Ltd. All rights reserved.
doi:10.1016/j.cemconcomp.2010.03.005

workability are also important factors that should be considered in the construction engineering. While HPFRCC is inexpensive compared to PCM and the surface coating resin, a further cost reduction is possible by a decrease in the fiber content. Lower fiber amounts would also reduce the viscosity and the yield value of HPFRCC, which would lead to better workability. On the other hand, reducing the amount of fiber may decrease the ductility and impermeability of HPFRCC. Therefore, a proper amount of fiber in HPFRCC should be determined, taking into account the trade-offs between these various properties.

In this study, therefore, the corrosion protection performance of HPFRCC used as a repair material was investigated. HPFRCC with fiber contents ranging from 0.75% to 1.5% was overlaid on normal concrete (NC) substrates to simulate surface coating or patch repair in order to investigate the effects of fiber content and overlaying method on corrosion protection performance. After introducing multiple fine cracks into the specimens, they were set into a chamber where a chloride solution was sprayed on the specimens periodically to accelerate deterioration by steel corrosion. The chloride penetration depth and the degree of steel corrosion of these specimens were investigated. Specimens using PCM and monolithic NC specimens were also prepared for comparisons with the HPFRCC specimens.

2. Mechanical performance of HPFRCC

To clarify the effect of the fiber content on the basic mechanical performance of HPFRCC, uni-axial tensile tests were carried out.

2.1. Materials and mixtures

Table 1 shows the physical properties of the high strength polyethylene (PE) fiber used in this study. Table 2 shows mixture compositions of HPFRCC. Besides the typical volumetric fiber ratio of 1.5% for HPFRCC [8], mixtures with smaller fiber ratios of 1.0% and 0.75% were used. The cement used was a high early strength Portland cement, and as the aggregate silica sand with a diameter range of from 100 to 200 mm was used. The additives used were a high range water reducing agent (polycarboxylate-based type) and a viscosity modifying agent (methylcellulose).

2.2. Specimens

For the uniaxial tension tests, dumbbell-shaped specimens shown in Fig. 1 were used following the JSCE standard [1]. An $80 \times 30 \times 30$ mm section in the middle part of the specimen is the gauge area where displacement is measured during the tensile test. The specimens used for the compressive test were 50 mm in diameter and 100 mm in length. Four of dumbbell-shaped specimens for the uniaxial tension test and three of compressive test specimens were prepared for each of the three types of mixtures. All the specimens were demolded 2 days after casting, and cured in water at 20 °C for about 2 weeks until the loading test was conducted.

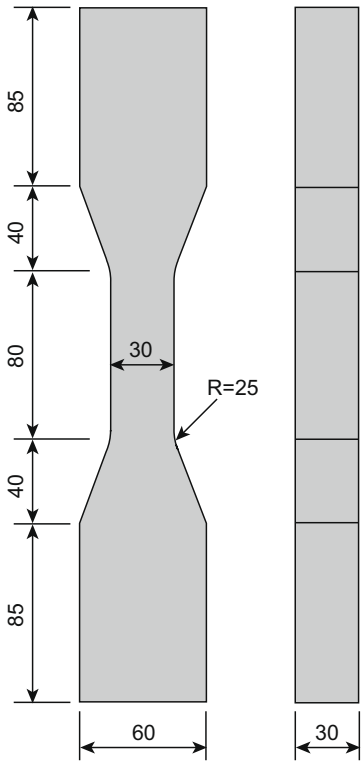

Fig. 1. Uniaxial tension test specimen [1] (unit: mm).

Table 1
Mechanical and geometrical properties of PE fiber.

Diameter (mm)	Length (mm)	Density (g/cm^3)	Tensile strength (GPa)	Young's modulus (GPa)
0.0012	12	0.97	2.6	88

2.3. Uniaxial tension test

The loading apparatus used for the uni-axial tensile test is shown in Fig. 2. Following the JSCE standard [1], the lower end was fix-supported and the upper end was pin-supported. Displacement transducers were set with a gauge length of 80 mm. The loading was controlled based on the displacement.

The loading was paused when the strain reached 0.2%, 0.5%, and 1.0%, respectively, the number of cracks was counted and the crack width was measured using a microscope (×50) and an image analysis system, with the displacement being held constant. Additionally, the number and the width of the cracks were determined again after unloading the specimens from the loading apparatus.

2.4. Properties of HPFRCC in a fresh state

Table 3 shows the air content and the mortar flow of each of the HPFRCC mixtures. Here, following the JIS R 5201 [9], the flows of

Table 2
Mixture compositions of HPFRCC.

	W/C	W (kg/m^3)	C (kg/m^3)	Silica sand (kg/m^3)	Fiber (kg/m^3)	HRWRA (kg/m^3)	VA (kg/m^3)
HPFRCC-1.5%	0.3	342.0	1264.0	395.0	14.6	37.90	0.90
HPFRCC-1.0%	0.3	343.7	1270.4	397.0	9.7	38.09	0.90
HPFRCC-0.75%	0.3	346.3	1280.1	400.0	7.3	38.38	0.91

HRWRA: high range water reducing agent; VA: viscosity agent.

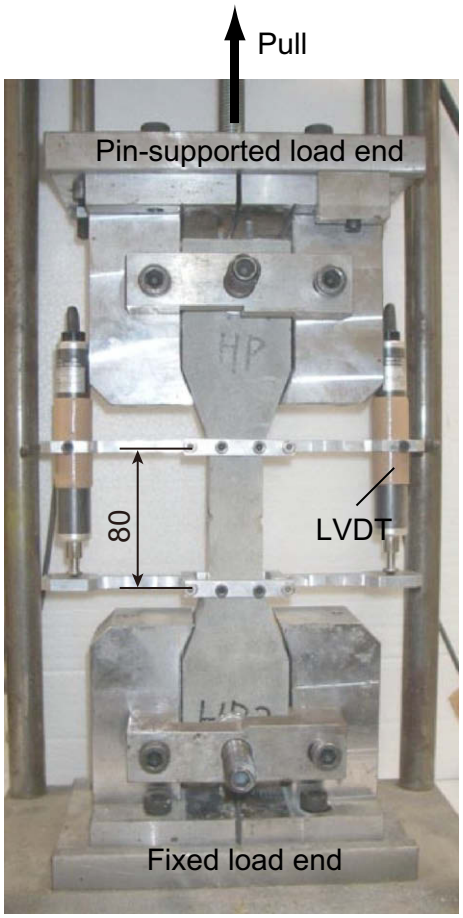

Fig. 2. Uniaxial tension test setup [1] (unit: mm).

Table 3
Flow and strength of HPFRCC.

	Air (%)	Mortar flow (mm)		Compressive strength (MPa)
		Before table drop	After table drop	
HPFRCC-1.5%	22	133	159	41.0
HPFRCC-1.0%	21	152	182	49.2
HPFRCC-0.75%	17	171	201	52.9

mortar were measured before and after dropping the flow table from a height of 10 mm 15 times in 15 s. Neither segregation of materials nor entanglement of fiber was observed in any of the mixtures. Table 3 shows that the flow increases by decreasing the fiber content of HPFRCC from 1.5% to 0.75%. In other words, decreasing the fiber content can increase the workability of HPFRCC, as expected.

2.5. Stress–strain relationship

Fig. 3 shows the stress–strain relationship of HPFRCC obtained from the uni-axial tensile tests using the dumbbell-shaped specimens. It should be noted that the large drops in stress when strain was 0.2%, 0.5%, and 1.0% are due to the pauses in the loading process in order to maintain the displacement. All the HPFRCC mixtures clearly exhibited pseudo strain-hardening characteristics. It can be recognized from this figure that the ultimate strain decreased with a reduction in the fiber content whereas there was no evident change in the tensile strength.

2.6. Cracks in HPFRCC

Figs. 4–7 show the average crack width, the number of cracks, the average crack spacing, and the maxim crack width of each of the HPFRCC specimens when the strain was 0.2%, 0.5%, 1.0%, respectively, and after the specimens were unloaded. In all the specimens, the average crack width was within 0.05 mm, and the number of cracks in the gauge area was more than 20. It should be noted here that one of the four HPFRCC-0.75% specimens ruptured during the loading test when the strain exceeded 1% and the crack width measurement was not possible for this specimen. Hence there is a drop in the average crack width of the HPFRCC-0.75% specimens in Fig. 4. The phantom line in Fig. 4 shows an estimated average crack width of the HPFRCC-0.75% specimens if the measurement had been carried out to all of the four specimens.

The specimens with a smaller amount of fiber had fewer cracks but a larger average crack width and maximum crack width when the strain was 1.0%. To be specific, the average crack width and the maximum crack width of HPFRCC-0.75% were 1.5 times larger than those of HPFRCC-1.5%. Furthermore, the HPFRCC-0.75% specimens unloaded after the tensile test had a much fewer number of cracks and a large average crack spacing. Therefore, the reduction in the ductility of HPFRCC specimens with lower fiber contents can be attributed to the smaller number of cracks generated during the tensile test.

Whereas the HPFRCC mixture with reduced fiber content was less ductile as shown above, all the mixtures investigated here had strain-hardening characteristics and exhibited multiple fine cracks. Therefore, the corrosion protection performance of all the three mixtures was investigated in the next section.

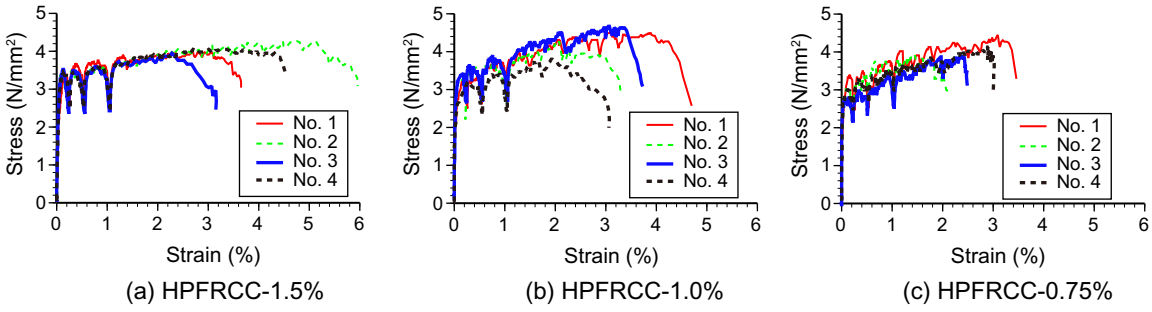

Fig. 3. Stress–strain relationship of HPFRCC with: (a) 1.5%, (b) 1.0%, and (c) 0.75% volumetric fiber content.

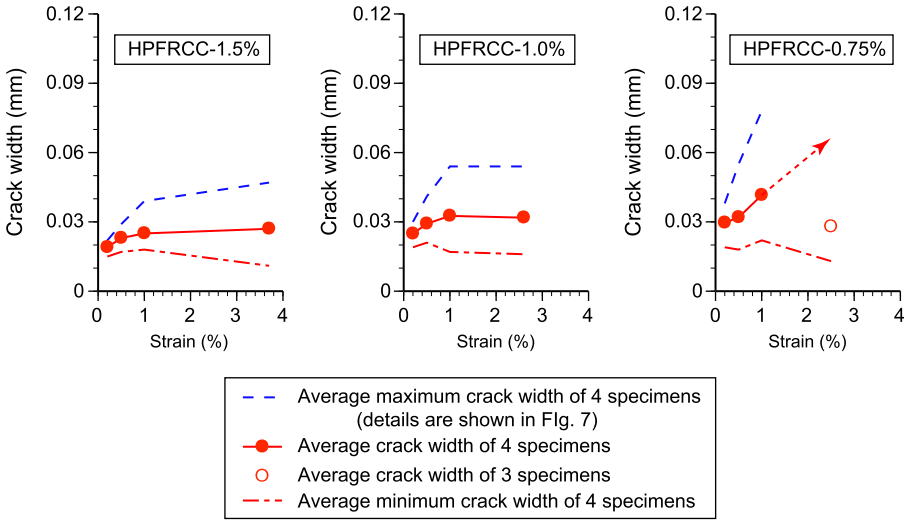

Fig. 4. The effect of fiber content on the average crack width.

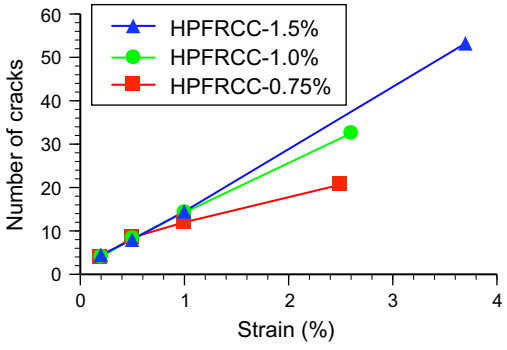

Fig. 5. The effect of fiber content on the number of cracks.

3. Corrosion protection by HPFRCC

It goes without saying that the chloride-contaminated concrete must be removed before the surface coating or the patching is applied on actual deteriorated structures. In this study, therefore, HPFRCC was overlaid on concrete specimens without chloride contamination, and the chloride solutions were then sprayed.

3.1. Materials and mixtures

Normal concrete was used for the substrate RC beam, and HPFRCC and polymer cement mortar (PCM) were used as the repair material. The mixture compositions of HPFRCC are the same as those shown in Table 2. Table 4 shows the mixture composition of NC; the maximum coarse aggregate size was 15 mm. PCM was a low-shrinkage type pre-mixed product of polyvinyl acetate–vinyl versatate (Va/VeoVA) designed for repair work. It should be noted that corrosion inhibitors were not used in this study even for the specimens that simulate a patch repair.

3.2. Specimens

Fig. 8 shows the specimens used for the investigation of corrosion protection performance. For all the specimens, D10 rebar was used. Monolithic specimens consist of NC. They were prepared in the form of RC beams with a cross section of 50 × 100 mm and a length of 1800 mm, which were then pulled to produce cracks (see Section 3.3) and cut into small specimens with a length of 150 mm. Surface coated specimens simulate a surface coating by HPFRCC. Initially, RC beams of NC with a cross section of 40 × 100 mm and a length of 1800 mm were prepared as the

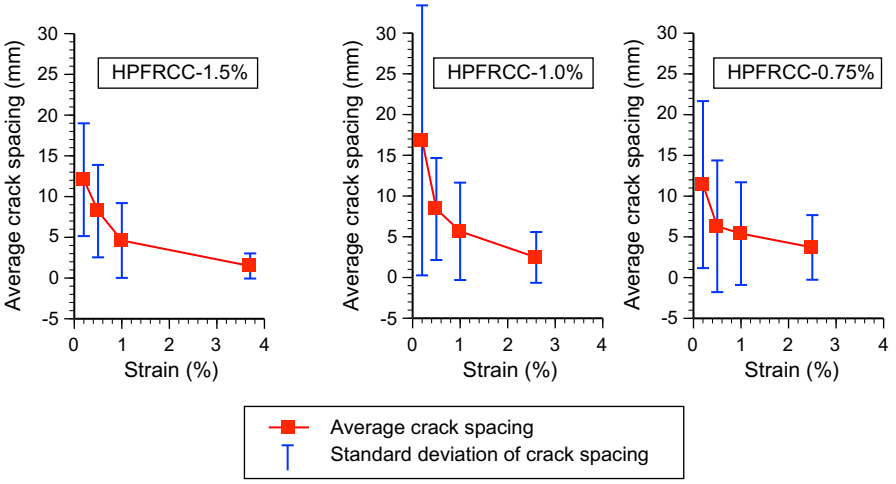

Fig. 6. The effect of fiber content on the average crack spacing.

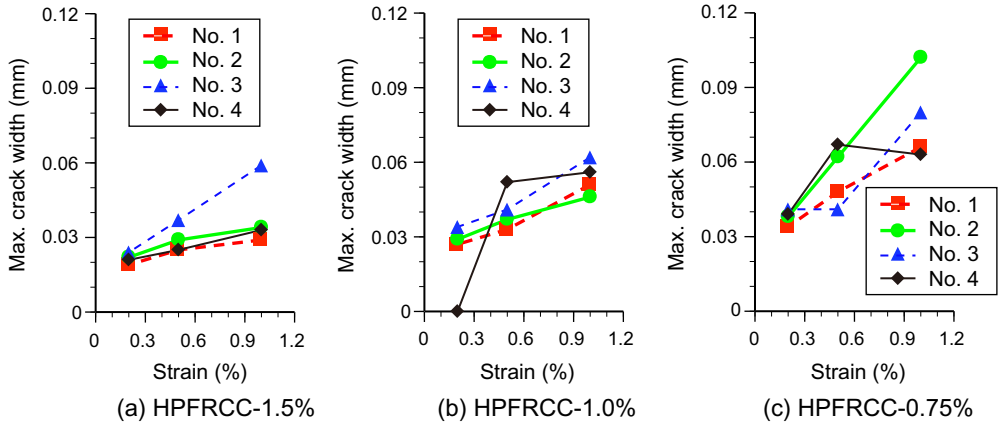

Fig. 7. The effect of fiber content on the maximum crack width.

Table 4
Mixture of NC.

	W/C	W (kg/m^3)	C (kg/m^3)	S (kg/m^3)	G (kg/m^3)	WRA (kg/m^3)
NC	0.55	180	327	810	920	0.8175

Table 5
Fresh properties and strength of each mixture.

	Air (%)	Mortar flow (mm)		Slump (mm)	Compressive strength (MPa)
		Before table drop	After table drop		
HPFRCC-1.5%	15.7	136	162		35.8
HPFRCC-1.0%	15.3	156	185		56.4
HPFRCC-0.75%	12.0	184	205		65.0
PCM					35.9
NC	3.9			58	47.1

substrate part, and HPFRCC or PCM was overlaid with a 10 mm thickness as a surface coating. The cover depth of reinforcing bars was 20 mm, the bars being arranged in the substrate part. Patched specimens simulate a patch repair using HPFRCC to restore a cross section of RC member to the backside of the reinforcing bars. Similarly to the surface coated specimens, RC beam of NC were prepared with a cross section of 40 × 100 mm and a length of 1800 mm as a substrate part, and HPFRCC or PCM was overlaid with a 35 mm thickness as a patching. While the cover depth was also 20 mm, the reinforcing bars were arranged in the patching part.

On the surface of the substrate part of NC on which HPFRCC or PCM was to be overlaid, a paper sheet immersed with a setting retarder was placed just after the casting to delay the setting of cement on the concrete surface. On the next day, the surface mortar that has not hardened yet was washed away with water to expose the coarse aggregate, before applying HPFRCC or PCM thereon. This was to simulate the surface treatments that are usually required for the repair of RC structures, such as sandblasting, chipping, or water jet blasting. After demolding on the third day,

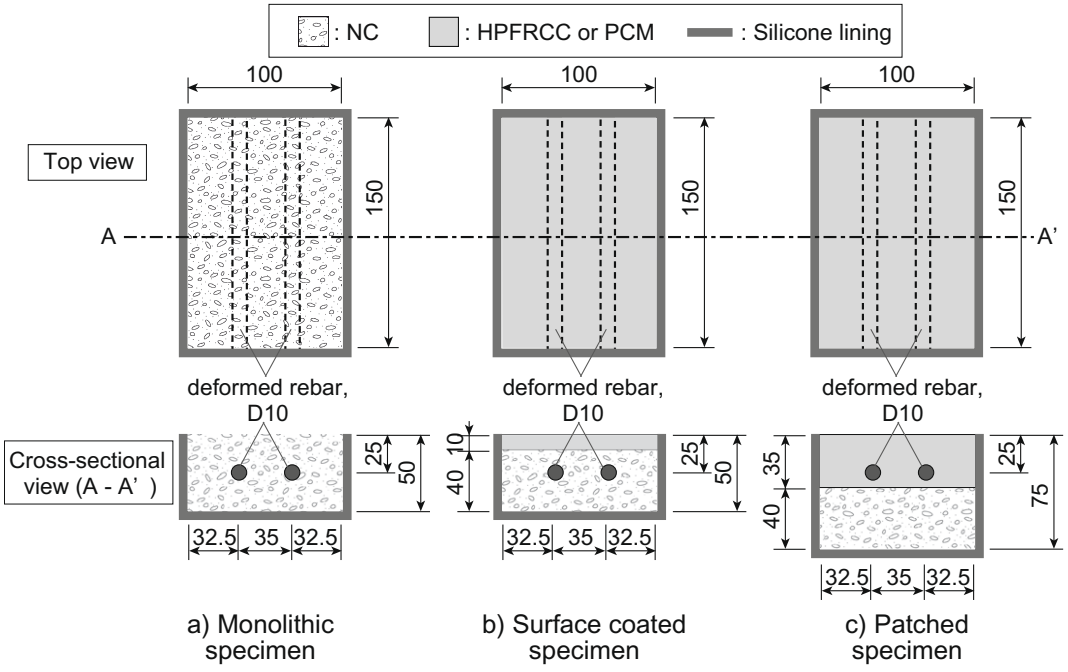

Fig. 8. Corrosion test specimens taken out from RC beams (unit: mm).

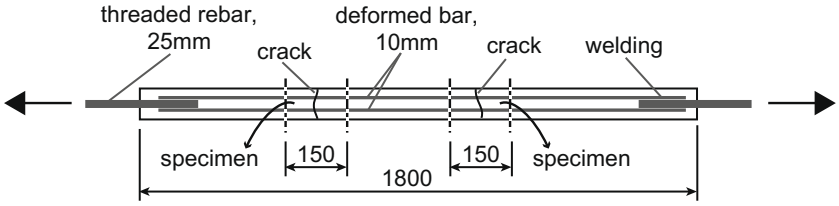

Fig. 9. Method of generating cracks in the beam (unit: mm).

Table 6
Maximum crack width in each specimen.

	Maximum crack width (mm)		
	Substrate	Repair	
		Rebar a	Rebar b
Monolithic specimen			
NC-1	–	0.36	0.47
NC-2	–	0.63	0.65
Surface coated specimen			
HPFRCC-1.5%-1	0.38	0.03	0.04
HPFRCC-1.5%-2	0.41	0.02	0.06
HPFRCC-1.0%-1	0.40	0.02	0.05
HPFRCC-1.0%-2	0.39	0.03	0.04
HPFRCC-0.75%-1	0.40	0.06	0.06
HPFRCC-0.75%-2	0.37	0.03	0.03
PCM-1	0.41	0.65	0.57
PCM-2	0.40	0.52	0.56
Patched specimen			
HPFRCC-1.5%-1	0.32	0.02	0.02
HPFRCC-1.5%-2	0.51	0.12	0.05
HPFRCC-1.0%-1	0.39	0.03	0.03
HPFRCC-1.0%-2	0.40	0.06	0.05
HPFRCC-0.75%-1	0.40	0.01	0.02
HPFRCC-0.75%-2	0.40	0.04	0.01
PCM-1	0.62	0.43	0.43
PCM-2	0.36	0.38	0.36

the specimens were supplied with water while curing at 20 °C for 2 weeks.

For the compressive strength tests, three cylindrical specimens of $\varphi 100 \times 200$ mm were prepared for each of the mixtures.

Table 5 shows the properties of each mixture. Compared to the results shown in Table 3, HPFRCC had a lower air content and a larger compressive strength. The flow values, however, were very similar to the results shown in the previous section, increasing with a decrease in fiber content.

3.3. Introduction of cracks

Fig. 9 shows the method of introducing cracks into the beam. D25 threaded-reinforcing bars that had been welded to both ends of the D10 reinforcing bars in the beams were pulled using a hydraulic jack in a uniaxial direction. The monolithic NC beams and the double-layer beams were loaded until the width of the cracks in NC reached about 0.4 mm. 150 mm long specimens that were to be used in the following corrosion tests were then cut out from the cracked parts of the beams as shown in Fig. 9.

Table 6 shows the precise crack width in both the substrate part and the repair part measured using a microscope with a magnification ratio of 175. The crack width shown here is that of the largest one of the cracks generated in each specimen. The crack widths were measured just above the two reinforcing bars, rebar a and rebar b. It should be emphasized that the crack widths in the double-layer HPFRCC specimens are almost the same as those of the dumbbell-shaped specimens, despite the presence of reinforcing steel and the double-layer structure (see Figs. 4 and 7). Detailed properties of cracks will be discussed in Section 3.7.

3.4. Acceleration of deterioration

To let the chloride penetrate into the specimens only from the upper side, the other five sides were sealed with silicone (see Fig. 8). Then a 3% chloride solution was sprayed on the specimens for 5 min every 6 h to accelerate the deterioration.

3.5. Measurement of chloride penetration depth

After 60 days of chloride spraying, the specimens were split parallel to the reinforcing bars to measure the chloride penetration depth. A solution of 0.1 N silver nitrate was sprayed on the fresh split surfaces to determine the chloride-contaminated area [10].

3.6. Measurement of steel corrosion

After the measurement of the chloride penetration depth, the reinforcing bars were taken out from the specimens. The outline of the corroded parts on the reinforcing bar was traced on a plastic sheet to measure the corrosion area using a planimeter. The corrosion area ratio was then calculated by Eq. (1), from the corrosion area and the nominal surface area of the reinforcing bars:

$$C_a = \frac{A_c}{A_0} \times 100(\%) \quad (1)$$

where C_a, corrosion area ratio; A_c, corrosion area (mm^2); and A_0, nominal surface area of reinforcing bar (mm^2).

After the corrosion area measurement, the rust was removed from the rebar using a wire brush. After that, the surface profile of the cleaned rebar was scanned using a non-contact laser type 3D scanner with a pitch of 0.6 mm in the longitudinal direction, to determine the corrosion depth and the cross-sectional loss of the rebar.

3.7. Crack distribution

Fig. 10 shows the crack distributions on the split surfaces of the specimens. A large crack runs transversely throughout the monolithic NC specimens and the PCM-overlaid specimens (Fig. 10c). In the HPFRCC-overlaid specimens, only one large crack was observed in the NC substrate part. At the same time, the HPFRCC layer had several fine cracks radiating from the point where the large crack in the NC substrate part reaches the interface between the substrate part and the overlaid part (Fig. 10a and b). This characteristic crack distribution was observed in both the HPFRCC surface coated and patched specimens. The high density of the cracks in HPFRCC part in the vicinity of the NC crack can be attributed to a reduced stiffness in the cross section of the substrate containing the crack as compared to other parts. Furthermore, this crack distribution proves a fine bond between HPFRCC and NC. An effect of the fiber content on the crack distributions was not observed in any type of the specimens that used HPFRCC.

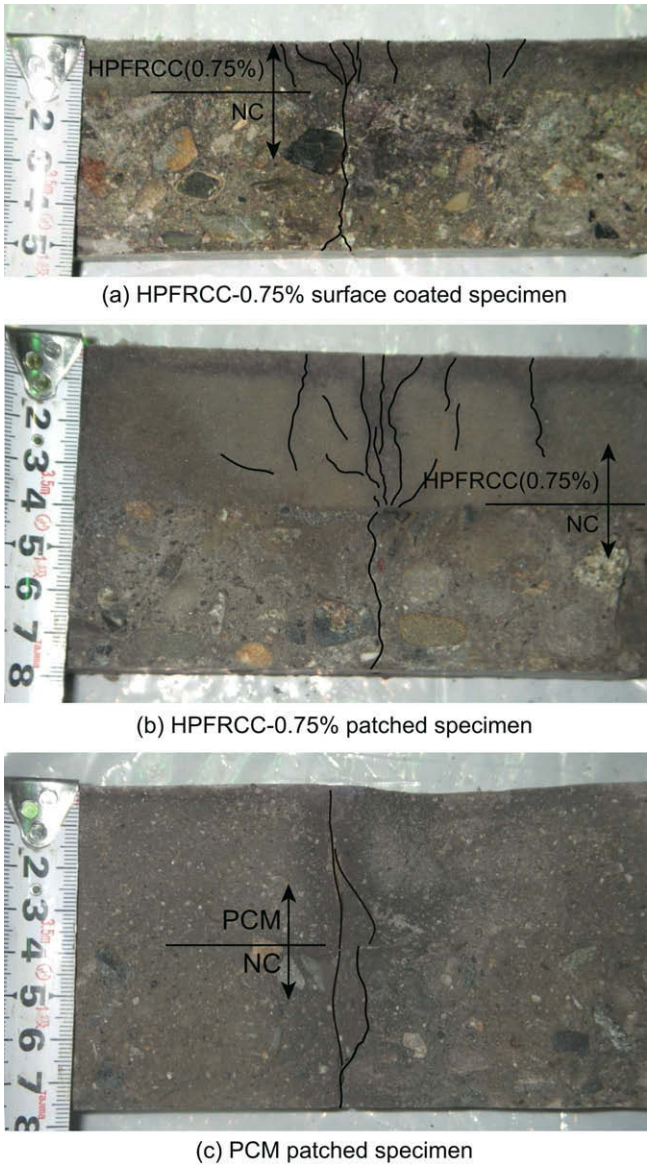

(a) HPFRCC-0.75% surface coated specimen

(b) HPFRCC-0.75% patched specimen

(c) PCM patched specimen

Fig. 10. Examples of crack distributions in specimens.

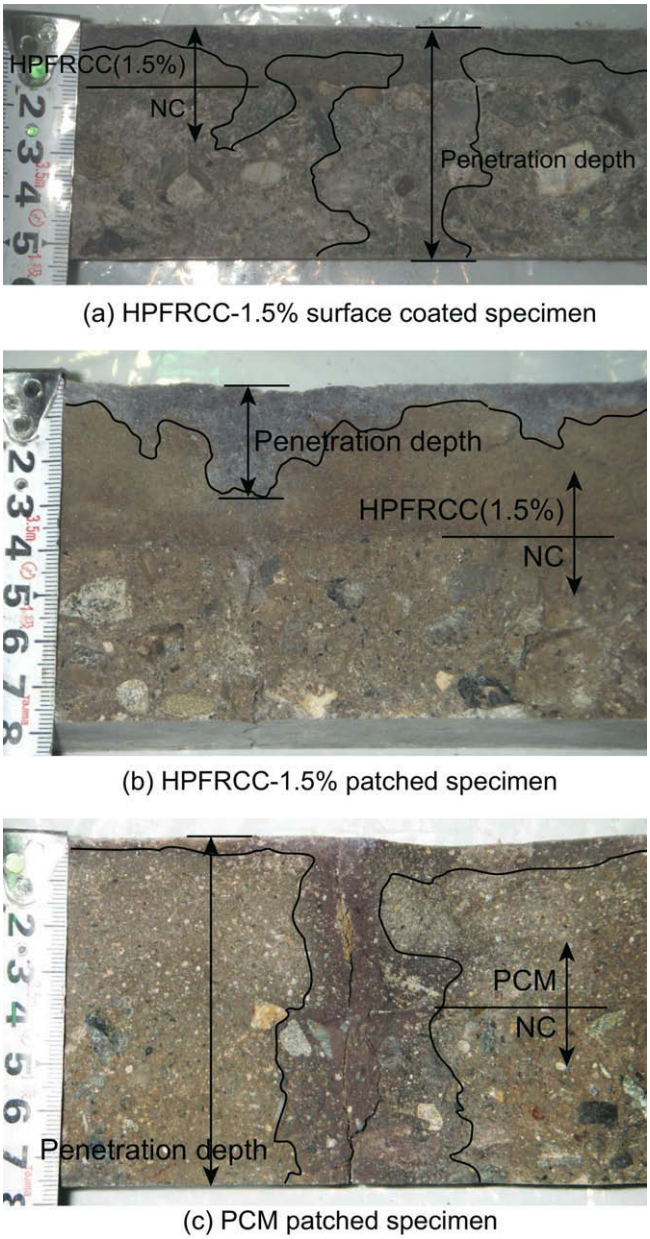

(a) HPFRCC-1.5% surface coated specimen

(b) HPFRCC-1.5% patched specimen

(c) PCM patched specimen

Fig. 11. Examples of chloride penetration profiles in specimens.

3.8. Corrosion penetration depth

Fig. 11 shows examples of the results of the chloride penetration test in which a silver nitrate solution was sprayed on the fresh split surfaces of the specimens. It is clear from this figure that the chloride has penetrated through the cracks. Fig. 12 shows the chloride penetration depths that were determined based on the color change caused by the silver nitrate solution. The penetration depth was measured at the crack(s), and in the case with the HPHFCC specimens, the penetration depth shown here is the largest one of the penetration depths measured at plural cracks.

In the NC monolithic specimens and the PCM-overlaid specimens, chloride had reached the bottom surface of the specimens through the cracks, while it had not in the HPFRCC-overlaid specimens. Besides, the penetration depth of the chloride in the longitudinal direction from the cracks in HPFRCC was smaller than that in NC, although no quantitative assessment was carried out here. Fig. 11b shows a very significant example of the chloride distribution in which the chloride penetration depth into the longitudinal direction is larger in NC substrate part than that in HPFRCC-overlaid part being directly sprayed with a chloride solution. The reasons for this are a very small crack width as a result of the bridging by fibers and a small water-binder ratio [3].

Whereas the chloride had reached the bottom surface of the specimen through the cracks in the PCM-patched specimens, the chloride penetration depths were as small as 25–45 mm in the HPFRCC-patched specimens (see Fig. 12c). It has been reported that the threshold crack width is 50–100 μm for water permeability [11,12] and 200 μm for chloride permeability [13,14]. The width of the cracks generated in the HPFRCC in this study was smaller than 100 μm in most of the specimens (see Table 6), and this is considered to be the reason for the small chloride penetration depth in the HPFRCC-patched specimens.

In all of the surface coated specimens including those with HPFRCC, the chloride had almost reached the bottom of the specimens (see Figs. 11a and 12b). This leads us to conclude that the 10 mm thickness of HPFRCC was insufficient to prevent the chloride from reaching the substrate. Once it reaches the substrate, it

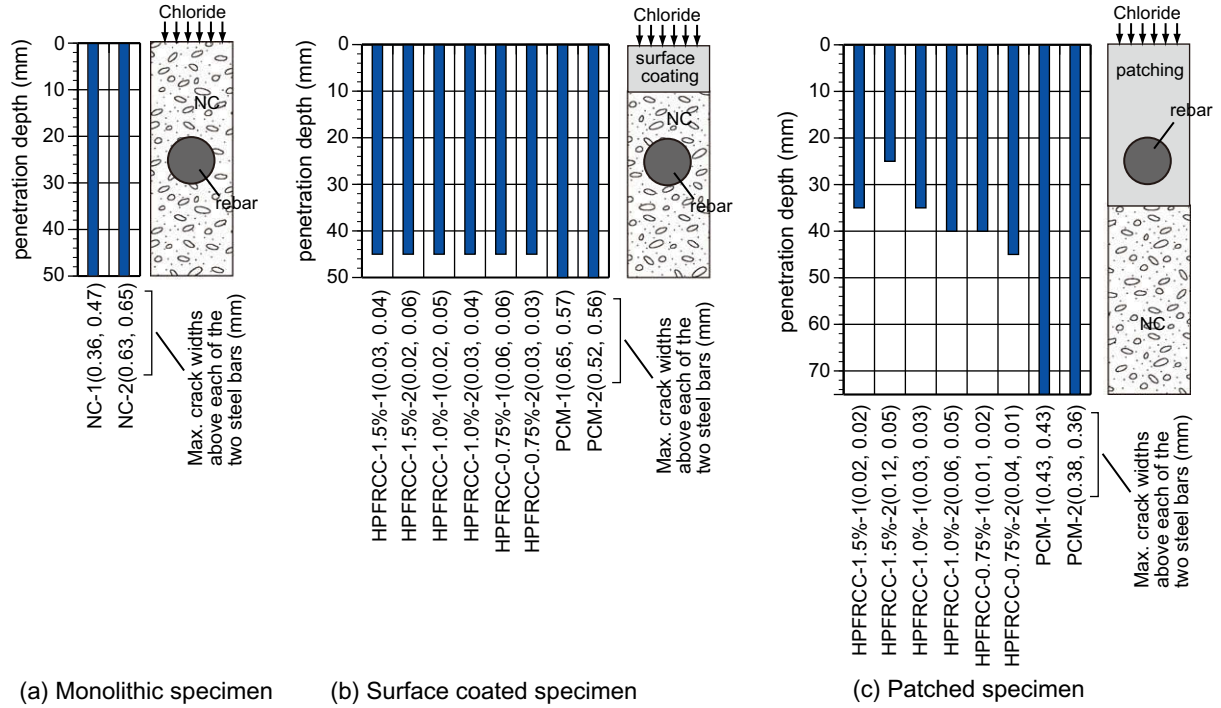

Fig. 12. Chloride penetration depth in specimens.

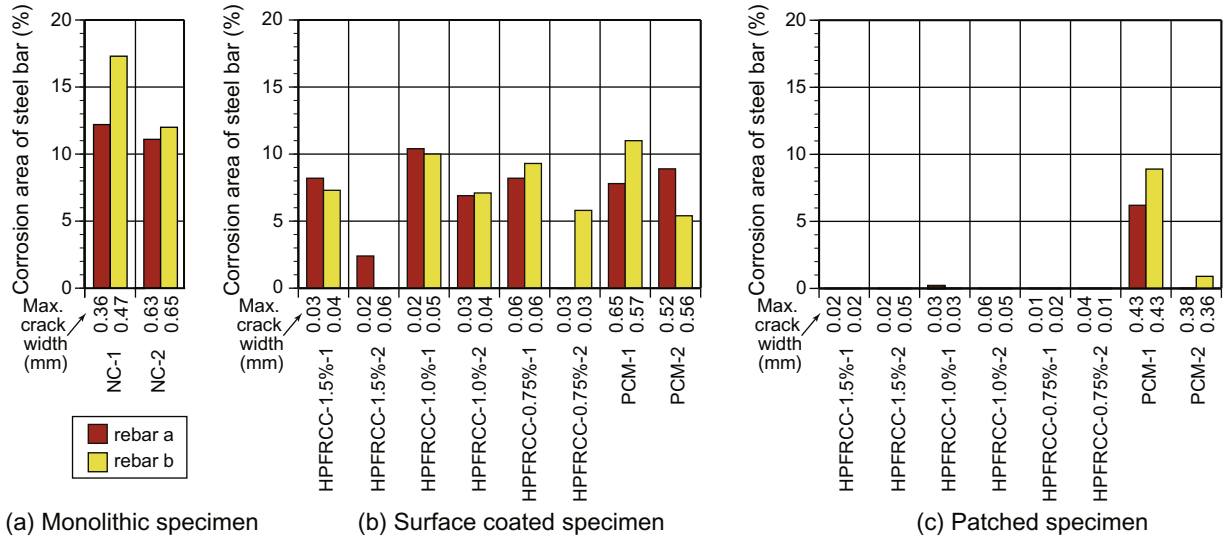

Fig. 13. Corrosion areas on the two steel rebars in each specimen.

can penetrate into the substrate concrete quickly through the wide cracks and the less dense microstructure due to high water–cement ratio.

3.9. Corrosion of reinforcing bar

Fig. 13 shows the ratio of corrosion area on the reinforcing bars. Since two bars were arranged in each specimen, two results are shown for each specimen in the figure. In the NC monolithic specimens with large cracks, the ratio of corrosion area on the reinforcing steel was relatively large (see Fig. 13a). This is attributable to the large chloride penetration depths in these specimens as shown in Fig. 12.

As for the surface coated specimens, corrosion was observed in almost all the bars, regardless of the type of overlaid mixture (see Fig. 13b). This is attributable to the large chloride penetration depth. Moreover, it is supposed that the large crack opening in the substrate NC part caused to create a debonding crack between the reinforcing bars and NC, allowing the chloride to penetrate farther along the interface between rebar and concrete.

The PCM-patched specimens failed to show sufficient corrosion prevention performance. As shown in Fig. 13c, the corrosion area ratios of the reinforcement in a PCM-patched specimen were as large as from 6% to 9%, whereas these values were smaller than those of the monolithic NC specimens. In contrast, the HPFRCC-patched specimen did prevent the steel corrosion, although it

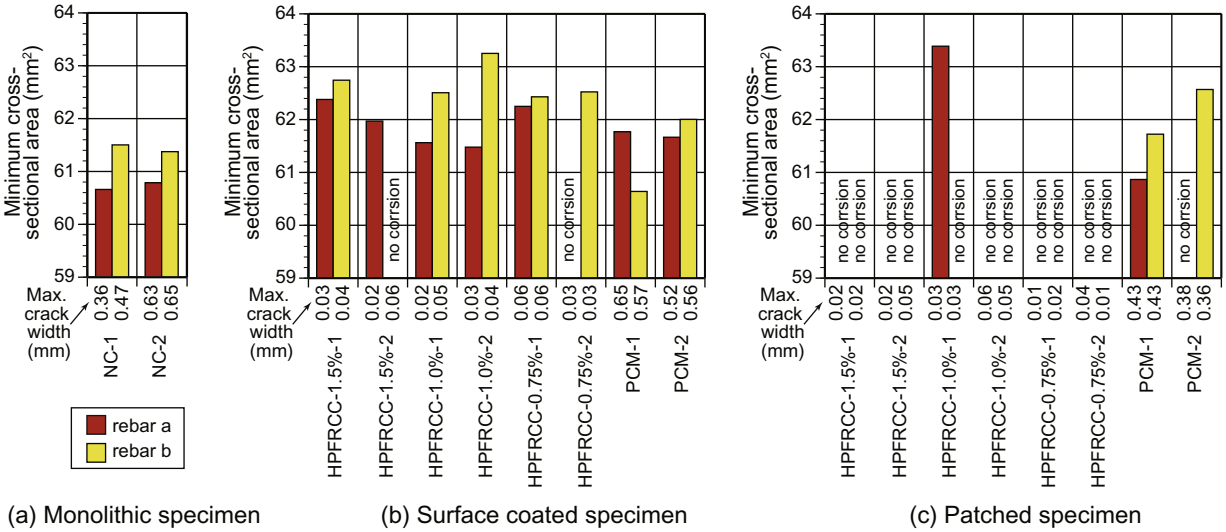

Fig. 14. The minimum cross-sectional area of each rebar.

suffered from slightly deeper chloride penetration as mentioned in the previous section (see Fig. 12c). The reason why the reinforcing bars did not corrode in HPFRCC-patched specimens even though the chloride penetrated beyond the bars could be assumed as follows: The chloride concentration around the bars is very small due to the very small crack width as described above. In addition, the generation of fine multiple cracks results in a smaller fracture area between the matrix and the steel. Furthermore, the matrix with the low water–cement ratio plus the viscosity agent made the microstructures tight at the interfacial zone between the matrix and the steel due to the low bleeding, resulting in the low supply of oxygen and water. Further, it is obvious from Fig. 13c that the fiber content in HPFRCC did not affect the corrosion prevention performance, even if it was halved from 1.5% to 0.75%.

The strength of the reinforcing bar is largely dependent on the minimum cross-sectional area of the bar. Therefore, Fig. 14 shows the minimum cross-sectional area of each corroded rebar calculated from the cross-sectional area distribution obtained using a 3D scanner. Here, the cross-sectional area profiles of the bar without corrosion were not measured. It should be noted that the bars used in this study were deformed bars with the mill scale and that there are large variations in the cross-sectional area of bars even without corrosion. Similarly to the corrosion area ratio, the loss of the cross-sectional area was the largest in the NC monolithic specimens (see Fig. 14a). As for the surface coated specimens, it can be recognized that the corrosion progressed into the depth direction from the steel surface even though the HPFRCC was overlaid on the substrate (see Fig. 14b). On the contrary, hardly any cross-sectional area loss of bars was detected in the HPFRCC-patched specimens (see Fig. 14c), which again confirms the high applicability of HPFRCC as a patch repair material.

As demonstrated above, the corrosion protection performance of HPFRCC was hardly affected by the fiber content, while the mechanical performance was affected significantly. This may be attributable to the difference in the strain of the specimen in each test. The average strain of all the specimens sprayed with chloride ranged from 0.2% to 0.3%, while it was as large as or larger than 2% in the uni-axial tensile test. It should be emphasized here that the number and width of the cracks were hardly affected by the fiber content when the strain was within 0.3%, as shown in Figs. 4–7. This resulted in the superior corrosion protection performance of all the HPFRCC mixtures when they were used as a patch repair material.

It can be concluded, therefore, that HPFRCC is effective as a chloride-resistant patch repair material, even with a fiber content that is less than a normal amount, provided it is applied with an appropriate thickness (i.e. to a depth beyond the reinforcing bar so that the bar is entirely embedded in HPFRCC). However HPFRCC used as a surface coating material, even with a sufficient amount of fiber, cannot be expected to provide a satisfactory chloride-resistant performance.

Another significant aspect is that a crack width of 0.4 mm, which was generated in the NC substrate part in this section, is large and unlikely to be seen in normal service conditions. Indeed, the reinforcing bars in the specimens were pulled until they yielded to form residual cracks in this study, i.e., the experiment was conducted under more severe conditions than those foreseen in actual applications. In addition, the application of repair materials to a structure already deformed by dead loads and creep may result in a smaller crack width in the repair material and much better durability. Therefore, the applicability of HPFRCC to in situ structures should be investigated.

4. Conclusions

This paper regards the corrosion protection performance of HPFRCC as a repair material. For the purpose of improving workability, the volumetric fiber content in HPFRCC was decreased from its usual rate of 1.5% to as low as 0.75%. In the first section of this paper, mechanical performances and crack patterns of HPFRCC mixtures with various fiber contents were investigated through uniaxial tension tests.

Using these mixtures, the applicability of HPFRCC as a repair material for preventing steel corrosion was investigated. For this purpose, two types of specimens were prepared to simulate repairs: surface coated specimens formed by a 10 mm thick HPFRCC layer overlaid on the substrate; and patched specimens formed by a 35 mm thick HPFRCC layer overlaid so that the reinforcement was completely embedded. Specimens using PCM and monolithic normal concrete (NC) specimens were also prepared for comparisons with the HPFRCC specimens. On these specimens, a chloride solution was sprayed to accelerate the chloride-induced corrosion of reinforcing steel. After being exposed to this environment, the chloride penetration depth and the corrosion of the reinforcing steel were investigated. The results obtained on this study can be summarized as follows:

(1) Decreasing the fiber content in HPFRCC from 1.5% to 0.75% clearly reduced the ultimate strain, while no clear decrease was observable in strength.
(2) With the strain resulting from the uniaxial tension test being 1.0%, the HPFRCC specimens with smaller fiber contents tended to have cracks with a larger mean crack width and a larger mean crack spacing.
(3) HPFRCC showed better chloride-resistant performance as compared to NC and PCM.
(4) Surface coating with HPFRCC did not prevent the corrosion of the steel in the substrate RC member.
(5) Patch repair with HPFRCC to depths beyond the backside of the reinforcement effectively suppressed chloride penetration and prevented reinforcement corrosion.
(6) Reducing the fiber content to 0.75% did not affect the corrosion preventing performance of HPFRCC as a patch repair material, and therefore both improved workability and high corrosion preventing performance were attained by decreasing the fiber content in HPFRCC.

References

[1] JSCE Concrete Committee. Recommendations for design and construction of high performance fiber reinforced cement composites with multiple fine cracks (HPFRCC). Concrete engineering series no. 82, July 2008. <http://www.jsce.or.jp/committee/concrete/e/hpfrcc_JSCE.pdf>.
[2] Lim YM, Li VC. Durable repair of aged infrastructures using trapping mechanism of engineered cementitious composites. Cem Concr Compos 1997;19(4):373–85.
[3] Sahmaran M, Li M, Li VC. Transport properties of engineered cementitious composites under chloride exposure. ACI Mater J 2007;104(6):604–11.
[4] Sahmaran M, Li VC, Andrade C. Corrosion resistance performance of steel-reinforced engineered cementitious composite beams. ACI Mater J 2008;105(3):243–50.
[5] Sahmarana M, Li VC. Durability of mechanically loaded engineered cementitious composites under highly alkaline environments. Cem Concr Compos 2008;30(2):72–81.
[6] Miyazato S, Hiraishi, Y. Transport properties and steel corrosion in ductile fiber reinforced cement composites. In: Proc. ICF, vol. 11, Torino; 2005.
[7] Kamal A, Kunieda M, Ueda N, Nakamura M. Evaluation of crack opening performance of a repair material with strain hardening behavior. Cem Concr Compos 2008;30(10):863–71.
[8] Yamada Y, Inaguma T, Kobayashi K, Fischer G, Rokugo K. Discussions of conditions for multiple cracking of HPFRCC based on Variability of strength properties. In: Proceedings of 8th international symposium on utilization of high-strength and high-performance concrete (8HSC-HPC), Tokyo, October 2008. p. 1113–8.
[9] JIS R 5201-2007. Physical testing methods for cement.
[10] Otsuki N, Nagataki S, Nakashita K. Evaluation of $AgNO_3$ solution spray method for measurement of chloride penetration into hardened cementitious matrix materials. ACI Mater J 1992;89(6):587–92.
[11] Aldea C-M, Shah SP, Karr A. Permeability of cracked concrete. RILEM Mater Struct 1999;32:370–6.
[12] Wang K, Jansen DC, Shah SP, Karr A. Permeability study of cracked concrete. Cem Concr Res 1997;27(3):381–93.
[13] Aldea CM, Shah SP, Karr A. Effect of cracking on water and chloride permeability of concrete. ASCE J Mater Civil Eng 1999;11(3):181–7.
[14] Hoseini M, Bindiganavile V, Banthia N. The effect of mechanical stress on permeability of concrete: a review. Cem Concr Compos 2009;31:213–20.